particles

MDPI

Review

Electron Screening in Laboratory Nuclear Reactions

Jelena Vesić

Jožef Stefan Institute, Jamova cesta 39, 1000 Ljubljana, Slovenia; jelena.vesic@ijs.si

Abstract: A thorough understanding of nuclear reaction rates at low energies is essential for improving our understanding of energy generation in stars and primordial and stellar nucleosynthesis. At low energies, fusion reactions between charged particles are strongly suppressed by the presence of the Coulomb barrier, which classically inhibits the penetration of one nucleus into another. The barrier penetration causes the cross section to have a steep energy dependence at low energies, making cross section measurements very challenging. Furthermore, little is known about the impact of surrounding electrons in stellar plasmas that are currently beyond the reach of experiments. As a result, measuring the bare cross sections as accurately as possible is essential. Reaction rate measurements at very low energies have been made possible in recent years by the development of high-current low-energy accelerators as well as enhanced target and detection methods. Nevertheless, the presence of atomic electrons, which alter the Coulomb barrier by screening the nuclear charge and increase the cross section at low energies compared to the case of bare nuclei, complicates these observations. A review of the experimental and corresponding theoretical work on laboratory electron screening performed so far will be presented.

Keywords: electron screening; nuclear astrophysics; charge-induced reactions; reaction rates

1. Introduction

The rates of nuclear reactions at extremely low projectile energies, much below the Coulomb barrier, are influenced by the solid-state properties of the targets. In laboratory studies of nuclear reactions, the nuclei are typically in the form of atoms or molecules. The electrons surrounding the interacting nuclei enhance the probability of tunnelling through the Coulomb barrier [1]. This, in turn, results in an increase in nuclear reaction rates when the projectile energy is low. The electron screening effect was originally investigated for its significance in dense astrophysical plasmas, where nuclear reaction rates can be enhanced by many orders of magnitude. The effect can be explained theoretically by considering the electron screening energy [1].

The reaction cross section $\sigma(E)$ drops nearly exponentially with decreasing energy E [1]:

$$\sigma(E) = \frac{s(E)}{E}\exp(-2\pi\eta), \tag{1}$$

where $S(E)$ is the astrophysical factor which varies slowly with energy, energy-dependent Gamow factor $\exp(-2\pi\eta)$ describes the s-wave transmission through the Coulomb barrier. $\eta = \frac{z_1 z_2 e^2}{4\pi\varepsilon_0\hbar\sqrt{\frac{2E}{\mu}}}$ is the Sommerfeld parameter, Z_1 and Z_2 are the nuclear charges of interacting nuclei, μ is the reduced mass (in atomic mass units) and E center of mass energy (in keV).

The electron clouds surrounding the interacting nuclei act as a screening potential, thus reducing the height of the Coulomb barrier and leading to a higher "screened" cross section $\sigma_s(E)$, than would be the case for bare nuclei, $\sigma_b(E)$ (see Figure 1). An approaching

Citation: Vesić, J. Electron Screening in Laboratory Nuclear Reactions. *Particles* **2024**, *7*, 834–855. https://doi.org/10.3390/particles7030050

Academic Editor: Armen Sedrakian

Received: 8 August 2024
Revised: 6 September 2024
Accepted: 10 September 2024
Published: 15 September 2024

projectile does not experience any repulsive Coulomb force until it passes beyond the atomic radius R_a. An exponential enhancement factor is defined as:

$$f_{lab}(E) = \frac{\sigma_s(E)}{\sigma_B(E)} = exp\left(\pi\eta\frac{U_e}{E}\right). \quad (2)$$

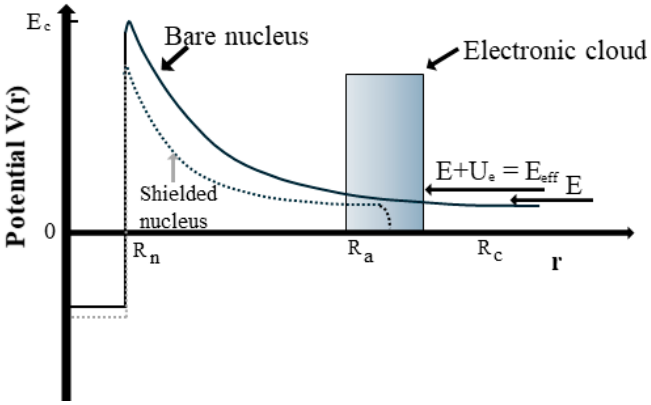

Figure 1. The effect of the atomic cloud on the Coulomb potential of a bare nucleus. R_c is a turning point, R_a is an atomic radius, R_n is a nuclear radius and U_e is a screening potential.

The screening effect was experimentally confirmed more than thirty years ago in gas target experiments [2]. This confirmation was based on the discovery of an exponential-like increase in the measured cross section as the projectile energy decreased, compared to the cross section expected for bare nuclei. From an atomic physics point of view (adiabatic limit) [1,3], the screening energy is given by the difference in atomic binding energies between the compound nucleus and the nuclei in the entrance channel [1,3,4]. Electron screening energies U_e have been determined for various nuclear reactions, mostly using Equation (2) to "match" the expression for the enhancement factor $f_{lab}(E)$ with the ratio of the measured cross section to the anticipated bare nuclear cross section (usually obtained by extrapolating cross sections from higher energies where screening effects are insignificant).

The effect of the surrounding charges on the reaction rate depends on the interplay between Coulomb and thermal energies [5,6]. This interplay is quantified by the parameter Γ:

$$\Gamma = \frac{(Ze)^2}{akT}, \quad (3)$$

where k is the Boltzmann constant, T is the temperature, Z is the charge of the nucleus, and a is the distance between the interacting nuclei. If the value of Γ is much smaller than 1, a "weak screening regime" occurs at high temperatures and/or low densities. On the other hand, when the density is high, specifically when $\Gamma >> 1$, a "strong screening regime" occurs. In a "strong screening regime", the most effective energy for nuclear reactions to happen (known as the Gamow peak energy) is significantly greater than the thermal energy. At high densities, where $\Gamma >> 1$, the bulk of the nuclei form a lattice (or quantum fluid). In this case, electrons can be treated as a uniform background. An enhancement factor can be derived by assuming that the interacting nuclei move while surrounded by a uniform electron cloud that neutralizes the nuclear charge. In this approximation, the enhancement factor can be written as $f_{sc} = e^{\frac{-U_e}{kT}}$ and the screening energy U_e can be calculated as the difference of electrostatic energies between the compound system with combined $(Z_1 + Z_2)$ charge and that of the two individual nuclei with charges Z_1 and Z_2.

If we consider a nearly perfect gas at a relatively low density and a weak screening regime (for which the average Coulomb energy between neighbouring nuclei is much

smaller than their thermal energy), the measure of the charged cloud surrounding each nucleus is given with the Debye radius R_D:

$$\zeta R_D = \left(\frac{kT\varepsilon_0}{4\pi\alpha\rho} \right)^{1/2}, \quad (4)$$

where α is the fine-structure constant and ρ is the number density of nucleons. ζ depends on the composition of the plasma and its degree of degeneracy [5–7]. Due to the effect of the screening clouds, the interacting nuclei with charges Z_1 and Z_2 feel a screened Coulomb potential $U_{sc} = \frac{Z_1 Z_2 e^2}{r} e^{\frac{-r}{R_D}}$ [5–7]. The tunnel process occurs at radii which are significantly smaller than the Debye radius. Thus, the exponential in the screened Coulomb potential $e^{\frac{-r}{R_D}}$ can be expanded to first order $e^{\frac{-r}{R_D}} = 1 - \frac{r}{R_D}$. Therefore, the effect of screening is a reduction of the Coulomb barrier by a constant screening energy $U_e = \frac{Z_1 Z_2 e^2}{R_D}$. The interacting nuclei in the plasma fuse with a slightly increased energy ($E + U_e$) and the enhancement factor equals to $f_{sc} = e^{\frac{-U_{sc}}{kT}}$.

Understanding the increased electron screening in metallic environments is crucial for comprehending strongly coupled astrophysical plasmas. The screening energies measured by many research groups for numerous metals exceed the theoretical predictions. The theory of electron screening in stellar plasma is still based on the physics model proposed by Salpeter in 1954 [6]. However, there have been substantial advancements in mathematical treatments since then. Since nuclear fusion reactions in plasma do not follow statistical equilibrium, the fusing nuclides may capture electrons from the plasma ("sea of electrons") during the fusion process, resulting in conditions similar to those observed in laboratory nuclear reaction investigations. The era of experiments on electron screening effects in terrestrial plasma has not yet started (although the future looks promising). Therefore, the typical approach is to first eliminate the screening effects caused by the laboratory and obtain the bare nuclear cross section σ_b. This cross section is subsequently adjusted to account for the solar plasma screening. Therefore, it is necessary to consider the distinct impacts of screening for the solar cross section σ_{solar} and the laboratory ones, σ_{lab}.

2. Electron Screening in the Laboratory

The impact of electron screening on low-energy fusion cross sections was first demonstrated in the late 1980s [2]. Despite extensive theoretical investigations and numerous experiments conducted over the past few decades, a theory that can account for the exceptionally high values of the screening potential required to explain the experimental data has not yet been established. Various experimental setups have been used, including different targets in the form of atomic and molecular gases, differently prepared metallic targets, and the use of both direct and inverse kinematics. A significant effort was put into eliminating errors in the extrapolation of data to zero energy and in calculating energy loss at ultra-low energies. However, current theoretical research in atomic physics has not yet provided a solution to this problem. This review aims to present a comprehensive overview of experimental studies of the electron screening effect and some theoretical studies. The list of reviewed reactions and corresponding screening potentials is given in Table 1.

2.1. d(d,p)t and d(d,n)^{3}He Reactions

Electron screening in deuteron–deuteron fusion reactions has been extensively studied due to the low Coulomb barrier and comparatively high cross sections. The D(d,p)t fusion reactions have been studied at cms (center of mass) energies E = 1.6 to 130 keV [8]. Electron screening potential U_e = 15 ± 5 eV was inferred. While the first D + d studies obtained using a gaseous target [8] were compatible with the adiabatic limit (U_e = 20 eV), screening energies obtained for various metal hosts differed among themselves and reached values of a few hundred eV.

The first study of the d(d,p)t reaction in Ti involved measuring thick target yields of protons emitted in the D(d,p)T reaction [9]. The incident deuteron energies were between 2.5 and 6.5 keV. The measured yields were compared with those obtained by using the parameterization of cross sections at higher energies. It was found that the reaction rates in Ti are slightly enhanced over those of the bare D + D reaction for E_d < 4.3 keV. The electron screening potential of U_e = 19 ± 12 eV was deduced.

The yields of protons produced during the D + D reaction in Pd, Au/Pd/PdO, Ti, and Au targets were measured at the incident energy ranging from 2.5 to 10 keV [10]. The measured yields were compared to the anticipated yields obtained from an extrapolation of the cross section and stopping power at higher energies. It was found that the enhancement factor of the d(d,p)t reaction is comparable for Ti and Au targets. The screening potentials of U_e = 250 ± 15 eV for the Pd target and 601 ± 23 eV for Au/Pd/PdO heterostructure target were measured. The variation of yields in different materials was explained by the diffusivity of deuterium in metals. Namely, the diffusivity of d in Pd and the Au/Pd/PdO heterostructure exhibited much higher values compared to Ti, and even more so when compared to Au. It was suggested that the high diffusivity in Au/Pd/PdO and Pd crystal lattice can lead to the development of a deuterium "fluidity" in the subsurface layer of the crystal lattice. It was also suggested that under the aforementioned conditions, this kind of environment could additionally promote the dynamic screening of deuteron–deuteron interactions, which arise from the coherent motion of the deuterons.

The thorough studies of electron screening in the d(d,p)t reaction have been performed by Raiola et al. [11–14]. The d(d,p)t reaction was studied for deuterated metals, insulators and semiconductors. The deuterated targets were produced via the implantation of low-energy deuterons. It was observed that the cross section for the fusion of two deuterons increases by more than an order of magnitude when deuterium is implanted into a metal. In the first study, a total of 29 deuterated metals and 5 deuterated insulators/semiconductors were studied to investigate the electron screening effect in the d(d,p)t reaction [11]. Significant differences have been observed in the metals V, Nb, and Ta (group 5), as well as in Cr, Mo, and W (group 6), Mn and Re (group 7), Fe and Ru (group 8), Co, Rh, and Ir (group 9), Ni, Pd, and Pt (group 10), Zn and Cd (group 12), and Sn and Pb (group 14) when compared to measurements conducted with a gaseous d_2 target. Conversely, a relatively small effect is observed in group 4 (Ti, Zr, Hf), group 11 (Cu, Ag, Au), and group 13 (B, Al), for the insulator BeO, and the semiconductors C, Si, and Ge. The absence of an elucidation of the seemingly novel characteristic of the periodic table was evident.

Raiola et al. [12] continued the studies of the d(d,p)t reaction using a deuterated Ta target. The electron screening potential energy of U_e = 309 ± 12 eV was obtained. The high U_e value was ascribed to the influence of the environment of the deuterons in the Ta matrix. Certain challenges to these measurements were addressed that are still nowadays valid. The first addressed challenge is that the U_e value is influenced by the energy dependence of the stopping power values of deuterium in Ta at energies significantly lower than the Bragg peak energy (E_d = 300 keV). At these energies, there was a lack of energy loss data, thus the values obtained from the compilation SRIM (Stopping and Range of Ions in Matter) [15] are based on extrapolations at $E_d \leq 100$ keV. Also, a notable distinction between a gas target and a solid target is that in the latter, channeling effects can occur. This meant that the deuteron beam could be directed by the lattice structure towards specific planes or axes, resulting in a higher likelihood of colliding with an interstitial atom such as deuterium. The critical angle for channeling is inversely proportional to the square root of the incident energy. Hence, the channeled flux is inversely proportional to the incident energy. Therefore, there is anticipated to be an increase in the cross section due to channeling that is directly proportional to $1/E$. However, this phenomenon was not observed. In addition, the Ta matrix in the experiment had a random orientation, and the crystalline structure was damaged by the powerful deuteron beam, resulting in significant dechanneling effects. Bonomo et al. [16] have stressed that a significant difference was noticed in d(d,p)t experiments conducted with a gaseous d_2 target as compared to

measurements in all metals except for the studied noble ones Cu, Ag, and Au. Insulators and semiconductors exhibited a relatively small effect in comparison. It was suggested that the substantial effect in metals can be explained by applying the classical Debye plasma screening [6] to the quasi-free metallic electrons. The cross section enhancement was attributed to the metallic valence electrons which may come closer to the deuteron and screen its charge more effectively than atomic electrons.

An even more extensive study of the d(d,p)t reaction was pursued by Raiola et al. [13]. A total of 58 samples, including deuterated metals, insulators, and semiconductors, were studied to investigate the electron screening effect in the d(d,p)t reaction. In comparison to the results obtained using a gaseous d_2 target, a significant effect has been observed in most metals, whereas a small effect is observed when using a gas target as well as employed insulators, semiconductors, and lanthanides. It was suggested that the significant cross section enhancements observed in metals can potentially be clarified by the application of the classical Debye plasma screening to the quasi-free metallic electrons. The data also included information regarding the hydrogen solubility in the samples. Comparing the U_e values with the periodic table revealed a constant pattern: for each group in the periodic table, the corresponding U_e values were either low (corresponding to "gaseous" values) for groups 3 and 4 and the lanthanides, or high for groups 2, 5 to 12, and 15. Group 14 stood out as an apparent anomaly in this regard: the metals Sn and Pb had a high U_e value, whilst the semiconductors C, Si, and Ge demonstrated a low U_e value, suggesting that high U_e values are characteristic of metals. Group 13 had a comparable scenario where B is an insulator, while Al and Tl are metals. The indication is further supported by the insulators BeO, Al_2O_3, and CaO_2. The metals in groups 3 and 4, as well as the lanthanides, exhibit a significant solubility in hydrogen, approximately equal to one. Consequently, they also functioned as insulators. Metals with measured high U_e values were known to have low solubilities, although specific values at room temperature were only known for a limited number of cases. This study revealed that the average solubility was approximately 12% while maintaining the metallic properties of the sample. It was also stressed that obtaining more accurate measurements of the electron screening effects in deuterated materials necessitates the use of an Ultra High Vacuum system. Additionally, high-depth resolution analysis methods such as SIMS (Secondary-ion mass spectrometry), AES (Auger Electron Spectroscopy), and XPS (X-ray photoelectron Spectroscopy) were suggested to be required in situ to characterize the environment of the deuterium atoms at the surface with high precision.

The electron screening in the d(d,p)t reaction has been studied for the deuterated Pt at broad sample temperatures T = 20 °C–340 °C and for Co at T = 20 °C and 200 °C [14]. It was found that the enhanced electron screening decreases with increasing temperature. The data represented the first instance of temperature dependence of a nuclear cross section. The screening effect for the deuterated Ti was also measured for a broad range of temperatures at T = −10 °C–200 °C; above 5 °C, the hydrogen solubility dropped to values far below 1 and a large screening effect became observable. The solubility decreased with temperature and all metals of groups 3 and 4 and the lanthanides showed a solubility of a few percent at a higher temperature. At this temperature (T = 200 °C), a large screening became observable.

Czerski et al. [17] suggested the diffusion coefficients or conductivity of the Al, Zr, and Ta materials may provide insight into the significant cross section enhancements. On the contrary, Raiola et al. [12] suggested that a clear pattern did not emerge, the arguments were that the diffusion coefficient for Zr is significantly smaller than that for Al and Ta, differing by at least three orders of magnitude. However, the reported U_e values in ref. [17] did not demonstrate this same tendency. Similarly, the conductivity of Zr is at least three times smaller than that of Al and Ta. Furthermore, Raiola et al. [13] observed a connection between electron screening potential and the Hall coefficient of the metallic host, while Kasagi et al. [18] suggested that screening potential decreases with increasing deuteron concentration.

At approximately the same period as Czerski et al. [17] and Raiola et al. [11–14], Kasagi et al. [18] measured excitation functions for proton yield in the d(d,p)T reaction in Ti, Fe, Pd, PdO, and Au targets. Incident energies were ranging from 2.5 to 10 keV. It was found that the reaction rate at lower energies significantly changes depending on the host materials. The most enhanced d + d reaction rates occurred in PdO. At an energy of 2.5 keV, the rate increased by a factor of fifty compared to the rate of bare nuclei, and the screening energy determined from the excitation function was 600 eV. It was concluded that the significant increase could not be solely attributed to electron screening but that indicates the presence of another crucial screening mechanism in solids. Furthermore, the reaction rate enhancement was found to be highly dependent on the type of host materials. The highest increase was observed in PdO, with Pd and Fe following the trend. The obtained screening energy values were $600 \pm 20 \pm 75$ eV for PdO, $310 \pm 20 \pm 50$ eV for Pd, $200 \pm 15 \pm 40$ eV for Fe, $70 \pm 10 \pm 40$ eV for Au, and $65 \pm 10 \pm 40$ eV for Ti (statistical and systematic errors are given). The significant screening energies observed in PdO, Pd, and Fe implied the presence of a novel mechanism that increases the reaction rate, despite the standard approach (adiabatic limit) which predicts that the low screening energy produced by electrons in metal should be only a few tens of eV. Also, a significant correlation has been identified between the screening energy and the deuteron density. A high screening energy was associated with a low density in the host material during the irradiation. It was suggested that the increased fluidity of the deuteron in the host is the reason for the higher values of electron screening potential, as density is connected to the mobility of deuterium atoms in the host, and greater mobility leads to lower density [18].

To investigate the influence of the metallic environment on the electron screening, the angular distributions and thick target yields of the ^{2}H(d,p)^{3}H and ^{2}H(d,n)^{3}He reactions were measured [19]. The deuterons were implanted in three metal targets (Al, Zr, and Ta), at a beam energy ranging from 5 to 60 keV. The screening potential energies U_e of 190 ± 15 eV for Al, 297 ± 8 eV for Zr and 322 ± 15 eV for Ta were obtained. The experimentally obtained results were one order of magnitude larger than the value $U_e = 25 \pm 5$ eV determined from a gas target experiment. A clear correlation between the screening energy and the target material was established. Further research on the ^{2}H(d,p)^{3}H reaction was performed by the same group [17] by studying the electron screening effect in the ^{2}H(d,p)^{3}H reaction using the previous three targets (Al, Zr, Ta) and two new targets (T, Pd). Targets were again implanted with deuterons. The electron screening potentials of 191 ± 12 eV, 295 ± 7 eV, 302 ± 3 eV, 296 ± 15 eV, and -20 ± 5 eV were obtained for AlD, ZrD_2, TaD, and $PdD_{0.2}$ targets, respectively.

The studies of the ^{2}H(d,p)^{3}H reaction were continued at very low energies in UHV conditions using deuteron-implanted Zr targets [20,21]. It was reported that the increase in enhancement factors seen with decreasing deuteron energy could not be solely attributed to the electron screening effect. It was also suggested that by incorporating an additional contribution from a single-particle threshold resonance, one can accurately explain the energy dependence of the experimental reaction yield. The screening energy obtained for the ^{2}H(d,p)^{3}H reaction and considering threshold resonance was significantly lower, namely $U_e = 105$ eV $\pm$ 15 eV compared to prior results, and agreed more closely with the theoretical estimate of 80 eV.

A series of experiments were performed to explore how surface contamination influences screening energies. The ^{2}H(d,p)^{3}H reaction cross section has been measured for deuteron energies below 25 keV in a deuterated Zr target under UHV conditions and controlled target surface contamination [22,23]. The increase of enhancement factors at lower energies was much lower than that determined before and could result not only from the electron screening effect but also from a 0^+ threshold resonance in ^{4}He. It was found that the enhancement factor increases noticeably in the first hours of the experiment, and then decreases until no screening effect is evident. It was also suggested that the cause of it might be a thick contamination that has covered the target surface. Initially, the target contamination was minimal (less than 1 atomic monolayer) and did not lead to energy

losses of projectiles. However, it did create crystal lattice defects that locally alter the band structure of the target.

Further experimental efforts on d(d,p)t cross section were performed in Ultra High Vacuum (UHV) conditions. Total cross sections and angular distributions of the ^{2}H(d,p)^{3}H and ^{2}H(d,n)^{3}He reactions were measured using a deuteron beam with energies ranging from 8 to 30 keV [24]. The cleanliness of the target surface has been confirmed by a combination of Ar sputtering and Auger spectroscopy. The online analysis method was also used to monitor the uniformity of the implanted deuteron densities. The screening energy for Zr obtained confirmed the high value obtained in a prior experiment of the same group [17] conducted under less optimal vacuum conditions.

To investigate the interplay between condensed matter physics and nuclear physics, Zirconium samples were exposed to different conditions and energy of deuteron beams in the accelerator system with a UHV at the eLBRUS laboratory, University of Szczecin [25]. X-ray diffraction (XRD) and positron annihilation spectroscopy (PAS) were used to analyze both irradiated and non-irradiated samples. The first method provided data on changes in crystal lattice parameters and the potential formation of hydrides due to dislocations formed during sample irradiation. The second method could identify the depth distribution of crystal defects, with a particular sensitivity to vacancies. The studied Zr samples were implanted with carbon and oxygen ions to create similar conditions that occur in nuclear reaction experiments and study their impact on the production of vacancies. It was suggested that the increased electron screening effect in the deuteron fusion process at very low energy may be due to the creation of many vacancies when samples are irradiated with deuterons. Carbon and oxygen impurities can impact this process by altering the depth distribution of vacancies and their diffusion. However, it was concluded that their influence on the strength of the electron screening effect is minimal. The experimental results demonstrate that irradiating Zr targets with deuterons results in high vacancy density which in turn leads to an increase in effective electron mass and consequently to the observed high electron screening effect in d + d reactions at low deuteron energies. This also explained the increase of the reaction yield shortly after cleaning the Zr target using argon sputtering under UHV conditions.

Further theoretical research by Czerski et al. [26] revealed a significant impact of the single-particle 0^{+} threshold resonance in ^{4}He. The resonance is supported by further considerations that are based on the weak coupling between the 2 + 2 and 3 + 1 clustering states of the compound nucleus ^{4}He. These arguments also predicted a large partial width for the internal production of electron-positron pairs, which leads to an overestimation of the proton width.

Most recently [27], electron emission in the d + d reaction supporting the existence of the single-particle threshold resonance in ^{4}He has been observed for the first time. The measured electron energy spectrum and the electron-proton branching ratio agreed well with the assumed electron-positron pair creation decay of the 0^{+} resonance state to the ground state. Additionally, the experimental energy spectrum was accurately reproduced by extensive Monte Carlo simulations [27].

The electron screening effect was studied in the d(d,n)^{3}He reaction in the ultralow deuteron collision energy range in the deuterated metals (ZrD_2, TiD_2 and $TaD_{0.5}$) [28]. The targets were made via magnetron sputtering of titanium, zirconium and tantalum in a gas (deuterium) environment. The detection of neutrons with an energy of 2.5 MeV from the d(d,p)t reaction was performed with plastic scintillator detectors. The energy dependence of the astrophysical S factor for the d + d reaction in the deuteron collision energy range of 2 to 7 keV was measured. The electron screening potential U_e of the interacting deuterons has been measured for the ZrD_2 (U_e = 205 $\pm$ 35 eV), TiD_2 target (U_e = 125 $\pm$ 34 eV), and $TaD_{0.5}$ target (U_e = 313 $\pm$ 58 eV).

2.2. ^{3}He(d,p)^{4}He Reaction

The ^{3}He(d,p)^{4}He reaction plays an important role in primordial nucleosynthesis of the light elements D, ^{3}He, ^{4}He, and ^{7}Li [4].

The reaction ^{3}He(d,p)^{4}He has been studied in the energy range of 5.9 to 41.6 keV using deuterium (d) projectiles and ^{3}He atomic gas target nuclei, as well as using ^{3}He projectiles and d_2 molecular gas target nuclei [2]. The results demonstrated a significant increase in cross sections, which may be described as almost exponential, as compared to the case where nuclei were not surrounded by electrons (bare nuclei). The electron cloud around the target nucleus, whether atomic or molecular, acts as a screening potential. As a result, the projectile effectively encounters a decreased Coulomb barrier for d projectiles and ^{3}He (atomic) target nuclei. An electron screening potential of $U_e = 120 \pm 10$ eV was obtained. The increase was about halved for the D(^{3}He,p)^{4}He reaction where a screening potential of $U_e = 66 \pm 4$ eV was obtained. The screening energy was expected to occur at lower energies due to the electron cloud in the d_2 molecule being at factor two greater distances than in the d atom.

The cross section measurements of the D(^{3}He,p)^{4}He reaction have been extended to include energy as low as $E_{cm} = 5.4$ keV [29]. The data had higher precision in comparison to prior research and validated the presence of electron screening. The combined analysis of the obtained dataset and past data [2,30] yielded an electron screening potential of $U_e = 123 \pm 9$ eV (A similar analysis of previous data for ^{3}He(d,p)^{4}He leads to $U_e = 186 \pm 9$ eV).

The fusion reaction ^{3}He(^{4}He,2p)^{4}He was studied at very low energy (for the first time the measurements were performed below the Gamow peak energy) at the Laboratory for Underground Nuclear Astrophysics (LUNA) accelerator facility located at the Gran Sasso National Laboratory (LNGS) [31,32]. It was concluded that enhancements at low energies are due to the electron screening effect. The measured screening potential $U_e = 294 \pm 47$ eV was close to the one from the adiabatic limit ($U_e = 240$ eV).

Angular distributions of cross sections and complete sets of analyzing powers for the ^{3}He(d,p)^{4}He reaction have been measured at five energies between $E_d = 60$ and 641 keV. The bare-nuclear cross section derived from the *R*-matrix parametrization was used to obtain the electron screening potential [33]. A screening potential of 177 ± 29 eV was reported.

Although the first 15 years of studies of electron screening were quite fruitful, the beginning of 2000 marked the start of the increased interest of the scientific community in this effect. One of the first performed measurements in the 2000s was of the D(^{3}He,p)^{4}He cross section in the energy range of 4.2 to 13.8 keV at the LUNA underground accelerator facility [34]. An electron screening potential energy U_e of 132 ± 9 eV, notably higher than the anticipated 65 eV value from an atomic physics model was obtained. In addition, it was concluded that the measured stopping power of the ^{3}He ions in the d_2 target (gaseous) agrees well with the standard compilation [35].

The cross section of the reactions ^{3}He(d,p)^{4}He and D(^{3}He,p)^{4}He has been experimentally determined for cms energies ranging from 5 to 60 keV and 10 to 40 keV, respectively. The experiments were conducted to measure the magnitude of the electron screening effect, resulting in the electron-screening potential energy values of $U_e = 219 \pm 7$ eV and 109 ± 9 eV [36]. These values are considerably larger than the corresponding values predicted by the adiabatic limit which results in $U_e = 120$ eV and 65 eV, respectively.

One of the sources of uncertainty is the bare nuclear cross sections required to deduce the experimental screening value. To eliminate this uncertainty, the Trojan Horse Method (THM) has been developed [37], which allows for an indirect determination of the bare nuclear cross sections at very low energies.

The cross sections of the ^{2}H(d,p)^{3}H and ^{2}H(d,n)^{3}He reactions have been measured via the THM that was applied to the quasi-free (QF) ^{2}H(^{3}He,p^{3}H)^{1}H and ^{2}H(^{3}He,n^{3}He)^{1}H reactions at 18 MeV off the proton in ^{3}He [38]. The value of $U_e = 13.4 \pm 0.6$ eV was extracted for ^{2}H(d,p)^{3}H while a value of $U_e = 11.7 \pm 1.6$ eV (below the adiabatic limit $U_e = 14$ eV for a molecular deuteron gas target) was extracted for ^{2}H(d,n)^{3}He reaction.

The fusion process between protons and deuterons has been studied by employing a proton beam with an energy of 260 keV and a graphite target implanted with deuterium [39]. The resulting product of the reaction, ^{3}He, mostly deexcites through the emission of γ-rays. However, in contrast to a γ ray, ^{3}He can also emit an electron with a discrete energy of 5.6 MeV. It was suggested that the probability of emission could be enhanced as a result of electron screening in graphite. Specifically, the internal conversion coefficient for a 5.6 MeV dipole transition in a helium nucleus is approximately 10^{-8}. In contrast, the measured coefficient was 10^4 times greater. Enhanced emission of 5.6 MeV electrons was ascribed to the electron screening, more specifically, to the electrons coming into the proximity of the nuclei and actively participating in the reaction.

The d(^{3}He,p)^{4}He reaction [40] was investigated in the ^{3}He$^+$ ion energy range from 16 keV to 34 keV using TiD targets with Miller indices of (111) and (100). It was shown that the target crystal structure had a significant influence on the reaction enhancement factor, namely the enhancement factor for E_{eff} = 6.51 keV was as twice as high for the TiD target with Miller indices (111). It was concluded that dependence of the enhancement factor for the reaction d(^{3}He,p)^{4}He as a function of energy is mostly influenced by solid-state effects, in particular by channeling. It was reported that high enhancement factors for the d(^{3}He,p)^{4}He reaction in the 16 to 22 keV energy range most likely point to the appearance of a novel mechanism that enhances the reaction's yield at lower energies. It was suggested that one of these effects is the aforementioned channeling of particles in crystalline structures.

The same group reported similar measurements of d(^{3}He,p)^{4}He reaction enhancement factor using targets ZrD with Miller indices (111), and (100) [41]. The measured enhancement factors of the d(^{3}He,p)^{4}He reaction were also higher for the ZrD target with a crystal structure characterized by the Miller index (100) than for the target with the Miller index (111), which was attributed to the contribution of channeling. In addition, a non-proportional increase of the enhancement factors for the d(^{3}He,p)^{4}He reaction in the energy range from 16 to 22 keV was explained with a low-lying resonance effect in ^{5}Li.

2.3. ^{6}Li(p,α)^{3}He, ^{6}Li(d,α)^{4}He, and ^{7}Li(p,α)^{4}He Reactions

The ^{7}Li(p,α)^{4}He reaction is one of the thermonuclear reactions involved in the stellar cycle of fusion of heavy elements in the universe [4].

The ^{6}Li(p,α)^{3}He and ^{7}Li(p,α)^{4}He reactions were investigated at energies from 10 to 65 keV using solid LiF targets [42]. The screening potential of U_e = 210 eV was measured in the case of ^{6}Li(p,α)^{3}He, which is slightly lower than the adiabatic limit of 240 eV, while U_e = 300 eV was measured in the case of ^{6}Li(p,α)^{3}He being somewhat higher. The results showed a significant increase caused by electron screening effects, following an exponential trend.

Shortly after the first electron screening studies reported in Refs. [2,42], at the beginning of the 1990s, reactions ^{6}Li(p,α)^{3}He, ^{6}Li(d,α)^{4}He, and ^{7}Li(p,α)^{4}He were investigated [30,43] in the cms energy range of 10 to 1004 keV. Each studied reaction employed hydrogen projectiles and solid LiF targets, as well as Li projectiles and molecular hydrogen gas targets. Electron screening had exponential effects on low-energy fusion cross sections in all studied cases. The impact of electron screening was slightly more pronounced when atomic target projectiles were used, as opposed to molecular H_2 or d_2 gas targets. Namely, for the ^{6}Li(p,α)^{3}He reaction, an electron screening potential of U_e = 440 ± 150 eV was obtained for the molecular hydrogen target and U_e = 470 ± 150 eV was obtained for the LiF target. For the ^{6}Li(d,α)^{4}He reaction, an electron screening potential of U_e = 330 ± 120 eV was obtained for the molecular deuterium target and U_e = 380 ± 250 eV was obtained for the LiF target. Last but not least, for the ^{7}Li(p,α)^{4}He reaction, an electron screening potential of U_e = 300 ± 160 eV was obtained for the molecular hydrogen target and U_e = 300 ± 280 eV was obtained for the LiF target. The possible impact of the isotope effect was also studied [43]. If the isotopic effect on electron screening is insignificant, all three reactions ^{6}Li(p,α)^{3}He, ^{6}Li(d,α)^{4}He, and ^{7}Li(p,α)^{4}He should have demonstrated equal enhancement

for each set of experimental data. The measurements fully confirmed this expectation since the deduced values of the screening potential energy U_e for all three reactions were equal within experimental error. For the ^{6}Li(p,α)^{3}He reaction, an electron screening potential U_e = 470 $\pm$ 150 eV was inferred for atomic and U_e = 440 $\pm$ 150 eV for the molecular hydrogen target. For the ^{6}Li(d,α)^{4}He reaction, U_e = 380 $\pm$ 250 eV was inferred for atomic and U_e = 330 $\pm$ 120 eV for the molecular deuterium target. For the ^{7}Li(p,α)^{4}He reaction, U_e = 300 $\pm$ 280 eV was inferred for atomic hydrogen and U_e = 300 $\pm$ 160 eV for the molecular hydrogen target. The obtained U_e was consistent with the results on the ^{3}He(d,p)^{4}He reaction [2,29]. Moreover, the U_e values for atomic targets were considerably larger than the expected value of U_e = 240 eV from the adiabatic model. It should be stressed that the adiabatic approximation, compared to other electron screening models, provides the largest screening potential theoretical estimates.

The ^{2}H(^{6}Li,α)^{4}He reaction was studied by applying the THM to the ^{6}Li(^{6}Li,$\alpha\alpha$)^{4}He three-body reaction [44]. The astrophysical $S(E)$ factor has been extracted in the energy range between 10–800 keV for the two cases of target and projectile quasifree break-up. The electron screening potential energy U_e = 320 $\pm$ 50 eV has been extracted in a model-independent way by comparing direct and THM data.

The cross section of the ^{6}Li(d,α)^{4}He reaction was measured for deuteron energies ranging from 50 to 180 keV [45]. The angular distributions and excitation function up to 1 MeV were analyzed using a distorted-wave Born approximation to assess the strength of a subthreshold resonance. At subcoulomb energy, this resonance significantly increases the astrophysical S factor by dominating the cross section. The reported electron screening energy of 130 $\pm$ 20 eV was significantly lower than the value reported in prior studies [30]. It was concluded that the difference may result from the fitting procedure, specifically from the polynomial fit of the measured cross section, used to determine the experimental value for the screening energy.

Kasagi et al. measured the α particle yields emitted in the ^{6,7}Li(d,α)^{4,5}He reactions in $PdLi_x$ and $AuLi_x$ targets [46]. The yields were measured as a function of the incident energy that was ranging from 30 to 75 keV. It was found that the reaction rate in Pd at lower energies is significantly increased compared to the rate anticipated for the cross section for the reaction involving bare nuclei. However, no such increase was observed in Au. A screening mechanism was implemented to accurately replicate the excitation function of the thick target yield for each of the metals. The inferred value of U_e for Pd was 1500 $\pm$ 310 eV, while for Au was just 60 $\pm$ 150 eV. It was again concluded that the observed improvements in the Pd example cannot be solely attributed to electron screening, indicating the presence of an additional and significant screening mechanism that occurs in metals (similar to [18]).

The electron screening effect was also studied in proton-induced reactions in ^{6,7}Li for different environments: Li_2WO_4 insulator, Li metal and $PdLi_x$ alloy [47,48]. The incident proton energies were between 30 and 100 keV. Large electron screening was found for Li metal (U_e = 1280 $\pm$ 60 eV) and $PdLi_{1\%}$ alloy (U_e = 3790 $\pm$ 330 eV) while a small effect, consistent with the adiabatic limit, was observed for Li_2WO_4 insulator (U_e = 185 $\pm$ 150 eV) [48]. Similar results have been found for the ^{6}Li(p,α)^{3}He reaction (U_e = 320 $\pm$ 110, 1320 $\pm$ 70, and 3760 $\pm$ 260 eV for Li_2WO_4, Li, and $PdLi_{1\%}$, respectively), supporting the hypothesis of the isotopic independence of the electron screening effect. These high values of U_e were again explained with the Debye plasma model applied to the quasi-free metallic electrons present in these materials. It was suggested that these results, together with prior studies of d(d,p)t [11–14] and ^{9}Be(p,α)^{6}Li in metals [49], confirm the Debye model scaling, where U_e is proportional to Z_t (the charge number of the target). The results were reanalyzed in ref. [47] using the *R*-matrix and polynomial fits, which were used to verify the bare astrophysical *S* factor with greater accuracy compared to earlier studies [48]. Using the newly obtained $S_b(E)$ data, a reassessment of the low-energy data for various targets, including Li_2WO_4 insulator, Li metal, and PdLix alloys, verified that the significant electron screening effects can be accounted for by applying the Debye plasma model to the quasi-free electrons in the metallic samples. The reanalysis also revealed that for the ^{7}Li(p,α)^{4}He reaction, the electron

screening energies are 1180 ± 60 eV for Li metal and 3680 ± 330 eV for $Pd_{94.1\%}Li_{5.9\%}$. The electron screening energy obtained for the $^{6}Li(p,\alpha)^{3}He$ reaction was U_e = 1280 ± 70 eV for Li metal, and U_e = 3710 ± 185 eV for $Pd_{94.1\%}Li_{5.9\%}$. The reanalyzed U_e values were around 100 eV lower but were within the error margin compared to the values stated in reference [48].

The $^{1}H(^{7}Li,\alpha)^{4}He$ reaction was studied in the energy range of 0.34 to 1.05 MeV using lithium beams. Hydrogen was diffused into Pd and PdAg alloy foils [50]. A significant electron screening effect was detected only when foils were subjected to tensile stress. There was no correlation found between the screening potential and the hydrogen content or Hall coefficient of the metallic host. The assertions by Kasagi et al. [46] that the screening potential decreases as the hydrogen concentration in metal increases could not be confirmed as the used concentrations were at least five times higher than the ones used by Kasagi et al. [46], and still, a greater screening potential was observed. Electron screening has been further studied in the fusion reaction $^{1}H(^{7}Li,\alpha)^{4}He$ using hydrogen-implanted Pd, Pt, Zn, and Ni targets at lithium beam energies ranging from 0.34 to 2.07 MeV [51]. A significant electron screening effect has been detected in all the targets.

2.4. $^{10}B(p,\alpha)^{7}Be$ and $^{11}B(p,\alpha)^{8}Be$ and $^{9}Be(p,\alpha)^{6}Li$ and $^{9}Be(p,d)^{8}Be$ Reactions

The $^{11}B(p,\alpha)^{8}Be$ reaction is the main destruction channel for the most abundant boron isotope in stars [4].

The fusion reactions $^{10}B(p,\alpha)^{7}Be$ and $^{11}B(p,\alpha)^{8}Be$ were investigated in a cms range of 17 to 134 keV by employing intensive proton beams and thick solid targets [52]. The low-energy data for the $^{11}B(p,\alpha)^{8}Be$ reaction exhibited an exponential increase (up to 1.9 times) in the astrophysical *S(E)* factor, which was attributed to electron screening effects. The low-energy data for the reaction $^{10}B(p,\alpha)^{7}Be$ showed an enhancement factor larger than 200, which could not be attributed solely to electron screening effects. The enhancement stems from the high-energy tail of an anticipated s-wave resonance at E_R = 10 keV. Regarding the electron screening potential, the deduced value was U_e = 430 ± 80 eV, obtained from the direct measurement of the $^{11}B(p,\alpha)^{8}Be$ *S(E)* factor under the hypothesis of no isotopic dependence of U_e. The adiabatic limit yields a theoretical value of 340 eV.

The THM was used to measure the $^{11}B(p,\alpha_0)^{8}Be$ reaction [53]. This was achieved by inducing the QF reaction $^{2}H(^{11}B,\alpha_0{}^{8}Be)n$ at a laboratory energy of 27 MeV. An enhanced data analysis technique has been utilized to derive the astrophysical *S(E)* factor from about 600 keV to zero energy. An electron screening potential of U_e = 472 ± 160 eV was reported.

The $^{10}B(p,\alpha_0)^{7}Be$ reaction has been measured for the first time at the Gamow peak using the THM applied to the $^{2}H(^{10}B,\alpha_0{}^{7}Be)n$ QF reaction [54]. The electron screening potential value has been determined to be 240 ± 200 eV using the measured bare-nucleus THM S(E) factor. The substantial error accounts for the uncertainties associated with the THM S(E) factor.

The excitation functions and angular distributions of the $^{9}Be(p,\alpha)^{6}Li$ and $^{9}Be(p,d)^{8}Be$ reactions were measured within the E_p = 16 to 390 keV energy range [49]. The data parametrization, especially at low energies, resulted in an electron screening potential energy of U_e = 900 ± 50 eV, which was significantly larger than the expected value of 240 eV based on the adiabatic limit.

Thick target α-yields from the $^{9}Be(p,\alpha)^{6}Li$ reaction were measured in the ultra-low energy range, between 18 and 100 keV [55]. It was obtained that the screening potential energy of beryllium is U_e = 545 ± 98 eV, which is significantly higher than the expectation from the adiabatic model of 264 eV. Nevertheless, from an experimental standpoint, the value is substantially less than other direct measurements (Zahnow et al., 900 ± 50 eV [49]).

Romano et al. [56] and Wen et al. [57] have examined the $^{9}Be(p,\alpha)^{6}Li$ reaction by employing the THM on the $^{2}H(^{9}Be,^{6}Li\alpha)n$ reaction. Wen et al. [57], for example, reported an electron screening potential of U_e = 676 ± 86 eV. The result has been extracted in a model-independent way by comparing the direct and THM data; Romano et al. [56] reported

only two points below the resonance region with poor resolution, so the results from Wen et al. [57] were used as representative of the THM results for comparison.

2.5. Reactions with Heavier Targets or Incident Nuclei

Electron screening in the ^{50}V(p,n)^{50}Cr reaction was investigated at E_p = 0.75 to 1.55 MeV in several environments: VO_2 insulator, V metal, and $PdV_{10\%}$ alloy. The reported screening energy for the metal and alloy were 27 ± 9 keV and 34 ± 11 keV, respectively, in comparison to the insulator. The reaction ^{176}Lu(p,n)^{176}Hf was also studied at comparable proton energies for a Lu_2O_3 insulator, Lu metal, and $PdLu_{10\%}$ alloy [58]. A narrow resonance was detected at E_{pr} = 0.81 MeV with a noticeable Lewis peak. The proton resonance energy shifted by 32 ± 2 keV and 33 ± 2 keV for the metal and alloy, respectively, compared to the insulator. The authors concluded that the electron screening effect happens throughout the periodic table and is not limited to reactions involving light nuclides that have been examined previously. Furthermore, it was concluded that two reactions involving neutrons in the exit channel show that electron screening affects the entry channel of the reaction and is not influenced by the charged particles in the exit channel. The U_e values were explained by applying Debye's plasma model to the quasi-free electrons in the metallic samples. The Debye model predicts a temperature dependence of the screening proportional to $T^{1/2}$, which was tentatively observed in [14]. The aforementioned observations, along with prior research on fusion reactions (d + d, Li + p and Be + p in metals) involving different nuclei, supported the Debye model's prediction that the electron screening potential scales with the nuclear charge of the target atoms. Moreover, it was anticipated using the same model that the α and β^+ decay rates would increase when radioactive sources are placed in metals at low temperatures [13,14]. Although Debye screening cannot be used for strongly coupled electron plasmas like metals at moderate temperatures, the idea has sparked significant interest [59]. The predictions based on the Debye-Hückel hypothesis about the temperature impact on the radioactive decay of implanted nuclei were not confirmed by the experiments. The measured values significantly deviated from their predicted values. Furthermore, their claims were in direct opposition to all other tests, especially the LTNO (Low-Temperature Nuclear Orientation) observations from the last decades. A material dependence would likely have been identified before, considering that nuclei crucial for nuclear technology have been studied in various chemical compounds, including pure metals, for many years. Most recently, the decay of ^{19}O(β^-) and ^{19}Ne(β+) implanted in niobium in its superconducting and metallic phases was measured using purified radioactive beams produced by the SPIRAL (The Système de Production d'Ions Radioactifs en Ligne) facility [60]. Half-lives and branching ratios measured in the two phases were consistent within a 1σ error bar.

No significant electron screening has been seen in the following proton-induced reactions: ^{55}Mn(p,γ)^{56}Fe, ^{55}Mn(p,n)^{55}Fe, ^{113}Cd(p,n)^{113}In, ^{115}In(p,n)^{115}Sn, ^{50}V(p,n)^{50}Cr, and ^{51}V(p,γ)^{52}Cr [51]. No change in the resonance energy between the metallic and insulator environments was seen in the examined (p,n) and (p,γ) reactions within the experimental error. The results disagreed with the data in ref. [58] that indicated significant electron screening potentials and resonance energy shifts in nuclear reactions with high-Z targets. It was suggested that the significant electron screening effect observed when hydrogen and deuterium nuclei are implanted into a metallic environment, or when hydrogen nuclei are absorbed from the gas phase and subjected to stress, may indicate that electron screening is influenced by the location of the target nuclei within a crystal lattice. The radiation damage from ion implantation creates crystal vacancies where hydrogen nuclei can be captured. Mechanical stress can lead to the movement of protons from regular interstitial positions to displaced interstitial positions in the crystal, where the hydrogen nuclei are once again captured physically [61].

The electron screening was investigated in the nuclear reactions ^{1}H(^{7}Li,α)^{4}He, ^{1}H(^{19}F,$\alpha\gamma$)^{16}O, and ^{2}H(^{19}F,p)^{20}F using a metallic environment as a probe, namely Pd foils that contained hydrogen [62]. A significant enhancement in the cross section due to electron screening in the first target (soft Pd foil) was not observed. However, in the second target (hard Pd

foil), a high electron screening potential for all three reactions was found, surpassing the theoretical predictions by an order of magnitude compared to the adiabatic limit. The data indicated that the discrepancy can be attributed to the influence of the host's crystal lattice structure and the location of the target nuclei in the metallic lattice on the electron screening potential. It was suggested that the different electron densities result in different screening potentials, as evidenced by the significant differences in Knight shifts measured in the targets. This suggested that the screening effect is not linked with the static electron concentrations around interacting nuclei, contrary to what the existing theory predicts.

Table 1. The list of studied reactions, corresponding adiabatic limits (U_e^{ad}) and experimentally deduced electron screening potentials (U_e^{exp}).

	Reaction	U_e^{ad}	U_e^{exp}	Remark	Reference
1.	D(d,p)T	20 eV	15 ± 5 eV	molecular target	[8]
2.	D(d,p)T	20 eV	19 ± 12 eV	Ti	[9]
3.	D(d,p)T	20 eV	250 ± 15 eV 601 ± 23 eV	Pd Au/Pd/PdO heterostructure target	[10]
4.	d(d,p)t	39 eV	309 ± 12 eV	Ta	[12]
5.	d(d,p)t	39 eV	440 ± 40 eV ≤30 eV ≤30 eV 350 ± 30 eV 220 ± 20 eV 350 ± 40 eV 450 ± 50 eV 200 ± 20 eV 450 ± 80 eV 43 ± 20 eV 140 ± 20 eV 320 ± 40 eV 83 ± 20 eV 400 ± 40 eV 220 ± 20 eV 220 ± 30 eV 840 ± 70 eV 800 ± 70 eV 23 ± 10 eV 390 ± 60 eV 200 ± 20 eV 87 ± 20 eV 340 ± 14 eV 220 ± 20 eV 700 ± 70 eV 330 ± 30 eV 40 ± 50 eV 61 ± 20 eV 440 ± 50 eV ≤30 eV ≤30 eV 52 ± 20 eV 45 ± 20 eV 60 ± 20 eV	Mg Al Ti V Cr Mn Fe Co Ni Cu Zn Y Zr Nb Mo Ru Rh Pd Ag Cd Sn Hf Ta W Re Ir Pt Au Pb BeO B C Si Ge	[11]

Table 1. *Cont.*

Reaction	U_e^{ad}	U_e^{exp}	Remark	Reference
		180 ± 40 eV	Be	
		440 ± 40 eV	Mg	
		520 ± 50 eV	Al	
		480 ± 60 eV	V	
		320 ± 70 eV	Cr	
		390 ± 50 eV	Mn	
		460 ± 60 eV	Fe	
		640 ± 70 eV	Co	
		380 ± 40 eV	Ni	
		470 ± 50 eV	Cu	
		480 ± 50 eV	Zn	
		210 ± 30 eV	Sr	
		470 ± 60 eV	Nb	
		420 ± 50 eV	Mo	
		215 ± 30 eV	Ru	
		230 ± 40 eV	Rh	
		800 ± 90 eV	Pd	
		330 ± 40 eV	Ag	
		360 ± 40 eV	Cd	
		520 ± 50 eV	In	
		130 ± 20 eV	Sn	
		720 ± 70 eV	Sb	
		490 ± 70 eV	Ba	
		270 ± 30 eV	Ta	
		250 ± 30 eV	W	
		230 ± 30 eV	Re	
		200 ± 40 eV	Ir	
		670 ± 50 eV	Pt	
6. d(d,p)t	39 eV	280 ± 50 eV	Au	[13]
		550 ± 90 eV	Tl	
		480 ± 50 eV	Pb	
		540 ± 60 eV	Bi	
		≤60 eV	C	
		≤60 eV	Si	
		≤80 eV	Ge	
		≤30 eV	BeO	
		≤30 eV	B	
		≤30 eV	Al_2O_3	
		≤50 eV	CaO_2	
		≤30 eV	Sc	
		≤30 eV	Ti	
		≤70 eV	Y	
		≤40 eV	Zr	
		≤40 eV	Lu	
		≤30 eV	Hf	
		≤60 eV	La	
		≤30 eV	Ce	
		≤70 eV	Pr	
		≤30 eV	Nd	
		≤30 eV	Sm	
		≤50 eV	Eu	
		≤50 eV	Gd	
		≤30 eV	Tb	
		≤30 eV	Dy	
		≤70 eV	Ho	
		≤50 eV	Er	
		≤70 eV	Tm	
		≤40 eV	Yb	

Table 1. *Cont.*

	Reaction	U_e^{ad}	U_e^{exp}	Remark	Reference
7.	d(d,p)t	39 eV	675 ± 70 eV 530 ± 40 eV 530 ± 40 eV 465 ± 38 eV 480 ± 70 eV 640 ± 70 eV 480 ± 60 eV ≤30 eV ≤50 eV 250 ± 40 eV 295 ± 40 eV 290 ± 65 eV 320 ± 50 eV 270 ± 75 eV 205 ± 70 eV 265 ± 70 eV 370 ± 70 eV 245 ± 70 eV 200 ± 50 eV 190 ± 50 eV 314 ± 60 eV 120 ± 60 eV 340 ± 85 eV 340 ± 80 eV 340 ± 70 eV 165 ± 50 eV 360 ± 80 eV 260 ± 80 eV 110 ± 40 eV ≤50 eV	Pt 20 °C Pt 100 °C Pt 200 °C Pt 300 °C Pt 340 °C Co 20 °C Co 200 °C Ti −10 °C Ti 50 °C Ti 100 °C Ti 150 °C Ti 200 °C Sc 200 °C Y 200 °C Zr 200 °C Lu 200 °C Hf 200 °C La 200 °C Ce 200 °C Nd 200 °C Sm 200 °C Eu 200 °C Gd 200 °C Tb 200 °C Dy 200 °C Ho 200 °C Er 200 °C Tm 200 °C Yb 200 °C C 200 °C	[14]
8.	^{2}H(d,p)^{3}H	80 eV	191 ± 12 eV 295 ± 7 eV 302 ± 3 eV 296 ± 15 eV −20 ± 5 eV	AlD ZrD_2 TaD $PdD_{0.2}$ CD	[17]
9.	d(d,p)t	39 eV	600 ± 20± 75 eV 310 ± 20± 50 eV 200 ± 15± 40 eV 70 ± 10± 40 eV 65 ± 10 ± 40 eV	PdO Pd Fe Au Ti	[18]
10.	d(d,p)t, ^{2}H(d,n)^{3}He	80 eV	190 ± 15 eV 297 ± 8 eV 322 ± 15 eV	Al Zr Ta	[19]
11.	^{2}H(d,p)^{3}H	80 eV	105 ± 15 eV		[20,21]
12.	d(d,n)^{3}He	80 eV	205 ± 35 eV 125 ± 34 eV 313 ± 58 eV	ZrD_2 TiD_2 $TaD_{0.5}$	[28]
13.	D(^{3}He,p)^{4}He ^{3}He(d,p)^{4}He	65 eV	123 ± 9 eV 186 ± 9 eV	combined analysis, including [2,30]	[29]
14.	^{3}He(d,p)^{4}He	65 eV	120 ± 10 eV	d_2 gas target	[2]
15.	^{3}He(d,p)^{4}He	120 eV	66 ± 4 eV		[2]
16.	^{3}He(^{3}He,2p)^{4}He	240 eV	294 ± 47 eV		[31,32]
17.	^{3}He(d,p)^{4}He	120 eV	177 ± 29 eV		[33]

Table 1. *Cont.*

	Reaction	U_e^{ad}	U_e^{exp}	Remark	Reference
18.	D(^{3}He,p)^{4}He	65 eV	132 ± 9 eV		[34]
19.	^{3}He(d,p)^{4}He	120 eV	219 ± 7 eV		[36]
20.	D(^{3}He,p)^{4}He	65 eV	109 ± 9 eV		[36]
21.	^{2}H(d,p)^{3}H	14 eV	13.4 ± 0.6 eV	THM	[38]
22.	^{2}H(d,n)^{3}He	14 eV	11.7 ± 1.6 eV	THM	[38]
23.	^{6}Li(p,α)^{3}He ^{7}Li(p,α)^{4}He	240 eV	300 eV 210 eV	LiF	[42]
24.	^{6}Li(p,α)^{3}He	240 eV	440 ± 150 eV 470 ± 150 eV	molecular target LiF	[30]
25.	^{6}Li(d,α)^{4}He	240 eV	330 ± 120 eV 380 ± 250 eV	molecular target LiF	[30]
26.	^{7}Li(p,α)^{4}He	240 eV	300 ± 160 eV 300 ± 280 eV	molecular target LiF	[30]
27.	^{6}Li(p,α)^{3}He	240 eV	470 ± 150 eV 440 ± 150 eV	atomic target molecular target	[43]
28.	^{6}Li(d,α)^{4}He	240 eV	380 ± 250 eV 330 ± 120 eV	atomic target molecular target	[43]
29.	^{7}Li(p,α)^{4}He	240 eV	300 ± 280 eV 300 ± 160 eV	atomic target molecular target	[43]
30.	^{2}H(^{6}Li,α)^{4}He	240 eV	320 ± 50 eV	THM	[44]
31.	^{6}Li(d,α)^{4}He	240 eV	130 ± 20 eV		[45]
32.	^{6,7}Li(d,α)^{4,5}He	240 eV	1500 ± 310 eV 60 ± 150 eV	$PdLi_x$ $AuLi_x$	[46]
33.	^{7}Li(p,α)^{4}He	240 eV	1280 ± 60 eV 3790 ± 330 eV 185 ± 150 eV	Li $PdLi_{1\%}$ Li_2WO_4	[48]
34.	^{6}Li(p,α)^{3}He	240 eV	320 ± 110 1320 ± 70 3760 ± 260	Li_2WO_4 Li $PdLi_{1\%}$	[48]
35.	^{7}Li(p,α)^{4}He, reanalysis	240 eV	3680 ± 330 eV 1180 ± 60 eV	$Pd_{94.1\%}Li_{5.9\%.}$ Li	[47]
36.	^{6}Li(p,α)^{3}He, reanalysis	240 eV	3710 ± 185 eV 1280 ± 70 eV	$Pd_{94.1}\%Li_{5.9\%}$ Li	[47]
37.	^{1}H(^{7}Li,α)^{4}He	240 eV	<600 eV <300 eV 1900 ± 600 eV 2800 ± 700 eV	Kapton Pd (no tensile stress) Pd (tensile stress applied) $Pd_{77}Ag_{23}$(tensile stress applied)	[50]
38.	^{1}H(^{7}Li,α)^{4}He	240 eV	4100 ± 1000 eV 2400 ± 1000 eV 2300 ± 500 eV 2800 ± 1300 eV	Ni Zn Pd Pt	[51]
39.	^{11}B(p,α)^{8}Be	340 eV	430 ± 80 eV		[52]
40.	^{11}B(p,α_0)^{8}Be	340 eV	472 ± 160 eV	THM	[53]
41.	^{10}B(p,α_0)^{7}Be	340 eV	240 ± 200 eV	THM	[54]
42.	^{9}Be(p,α)^{6}Li, ^{9}Be(p,d)^{8}Be	240 eV	900 ± 50 eV		[49]

Table 1. *Cont.*

	Reaction	U_e^{ad}	U_e^{exp}	Remark	Reference
43.	^{9}Be(p,α)^{6}Li	240 eV	545 ± 98 eV		[55]
44.	^{9}Be(p,α)^{6}Li	240 eV	676 ± 86 eV	THM	[56,57]
45.	^{50}V(p,n)^{50}Cr	11 ± 2 keV 17 ± 2 keV Debye model calculations	27 ± 9 keV (relative to VO_2) 34 ± 11 keV(relative to VO_2)	V $PdV_{10\%}$	[58]
46.	^{176}Lu(p,n)^{176}Hf	A shift in Lewis peak was observed	32 ± 2 keV (relative to VO_2) 33 ± 2 keV (relative to VO_2)	V $PdV_{10\%}$	[58]
47.	^{55}Mn(p,γ)^{56}Fe, ^{55}Mn(p,n)^{55}Fe, ^{113}Cd(p,n)^{113}In, ^{115}In(p,n)^{115}Sn ^{50}V(p,n)^{50}Cr ^{51}V(p,γ)^{52}Cr	No shift in resonance energy	/		[51]
48.	^{1}H(^{7}Li,α)^{4}He	240 eV	2.86 ± 0.19 keV	hard Pd foil	[62]
49.	^{1}H(^{19}F,αγ)^{16}O	2.19 keV	18.7 ± 1.5 keV	hard Pd foil	[62]
50.	^{2}H(^{19}F,p)^{20}F	2.19 keV	18.2 ± 3.3 keV 3.2 ± 1.9 keV	hard Pd foil soft Pd foil	[62]

3. Some Theoretical Investigations

The enhancement of the astrophysical S-factor for the d+^{3}He fusion process seen experimentally is demonstrated to be reproduced by the simple model of electron screening. The WKB (Wentzel–Kramers–Brillouin) method was used [63]. The effect of deuteron polarizability was also investigated and found to have a negligible contribution to the enhancement. The screening corrections were also applied to the ^{3}He(^{3}He,2p)^{4}He breakup reaction and data for the S-factor were reevaluated.

The three-dimensional Thomas-Fermi (TF) model was used to simulate the variation of the d(d,p)t cross section at low incident energies when the target deuterium nucleus is embedded in metallic or insulator environments [64]. It was concluded that even though the comparison of the computational results to experimental data demonstrated that the TF model could explain some increase in the low-energy cross section for the metallic host, a full explanation of the experimental results is still lacking.

The model reported in ref. [65] incorporated the dynamic treatment of the electron wave function evolution within the time-dependent Hartree-Fock (TDHF) scheme, while the motion of the nuclei was addressed classically. The screening effects in the d + H and d + He reactions were calculated and provided the effective screening energy U_e as a function of E for small internuclear distances. It was found that the obtained U_e values remain within the adiabatic limits, so they were unable to account for the higher screening energies observed in the aforementioned experiments.

A TDHF analysis of the screening effects in proton scattering on a molecular hydrogen target [66] revealed a significant dependence of the enhancement factor on molecular orientation. It was found that the screening effect is more pronounced for molecular targets than for atomic targets, mostly because of the reflection symmetry present in the latter. On the other hand, to explain high U_e potentials obtained in the d(d,p)t reaction, a theoretical effort has been made [67] to simulate the dynamics of reacting deuterons in a metallic lattice using an ab initio Hartree-Fock calculation of the overall electrostatic force between the lattice and the approaching deuterons through path integration. The calculations have demonstrated a migration of electrons from the metallic host to the deuterium atoms in the case of Li and Ta. However, it was concluded that to prevent further simplifications in the model, the use of a high-performance parallel supercomputer

would be necessary. The calculated values for the electron screening energies stayed clearly below the experimental ones. Furthermore, theoretical calculations were performed using the improved dielectric function theory [68], which enabled the derivation of a dependable deuteron–deuteron potential within the host metal. The theory included contributions from both quasi-free valence electrons and polarized bound electrons. The theory accurately explained the correlation between the screening energy and the target material, although it underestimated the actual values by approximately a factor of two.

Carraro et al. [69] calculated the enhancement factors for weakly screened thermonuclear reactions, explicitly accounting for their dependence on the velocity of the colliding particles (or simpler, corrections due to the non-uniform distribution of the electron cloud around the nucleus) and found that enhancements can be significantly smaller than those given by the adiabatic limit.

One has to stress that the recent paper from Iliadis [70] suggests that electron screening has different effects on nonresonant cross sections and resonance strengths and is not suitable for correcting measured resonance strengths using the same method as for correcting measured nonresonant cross sections. For narrow, low-energy resonances, the assumption of a constant screening energy is not valid and the radial dependence of the screening potential has to be considered, which leads to a significant reduction of screening on the resonance width [70].

In general, the possible uncertainties in the anticipated stopping powers might lead to a decrease in the effective energy of the reaction. As a result, the experimentally derived screening value would be higher than the actual value [71]. Indeed, discrepancies have been seen between theoretical calculations of stopping powers and the standard tabulation employed in the study of low-energy fusion data [72]. The theoretical improvements in treatments of ion energy loss at extremely low energies, along with independent experimental validation, are strongly needed.

4. Future Prospects

If it were feasible to directly measure reaction rates under solar plasma conditions, the discrepancy between observed and theoretical screening energies would no longer be of astrophysical significance. Laser-induced measurements of astrophysical S-factors were performed for the t+^{3}He [73] and d(p,γ)^{3}He [74] reactions (both of interest for Big Bang nucleosynthesis) at the OMEGA laser facility using inertially confined plasmas. These measurements were, however, performed under plasma conditions at which screening is expected to be negligible. Promising results could be obtained in future using the high-intensity lasers such as those in ELI-NP (Extreme Light Infrastructure-Nuclear Physics) [75].

The installation of the FISIC (Fast Ion Slow Ion Collisions) transverse beamline [76] will allow the crossing of the beams stored in CRYRING, thus opening up exciting opportunities for crossed-beam experiments. That enables the study of nuclear reactions between "bare" ion beams, unaffected by the electron screening, directly at the energies of astrophysical interest [77].

5. Conclusions

Charged-particle nuclear reactions occurring at energies below the Coulomb barrier are affected by screening and are also very important for nuclear astrophysics. However, reactions in the solar plasma and those in laboratories are affected differently due to their very different atomic environments; therefore, both screening mechanisms have to be understood.

A few instances have allowed for the measurement of the reaction cross sections at the energy that corresponds to the temperatures of star nucleosynthesis (laboratory measurements of the pp-chain reactions ^{2}H(p,γ)^{3}He and ^{3}He(^{3}He,2p)^{4}He, for example). Resolving the discrepancy between theoretical predictions and experimental observations of laboratory electron screening effects is crucial due to its astrophysical significance. This is necessary along with the ongoing remarkable efforts to lower the energies of laboratory

cross section measurements. Both enhanced theoretical investigations and independent experimental confirmation are required.

One may think that the substantial measured electron screening potentials are due to the experimental techniques that are very sensitive and prone to different kinds of systematic errors. However, one would probably rule out this possibility given the various groups, tools, and measurement techniques involved. More systematic and coherent experimental efforts are certainly needed. One of the most recent theoretical explanations explains high screening potential values observed with the clusterization effects in nuclear reactions, especially those involving light nuclei [78,79]. Improved efforts in theory are highly needed.

Funding: This research was funded by the Slovenian Research Agency and Innovation Grants no: P1-0102, I0-E005.

Conflicts of Interest: The author declares no conflict of interest.

References

1. Assenbaum, H.J.; Langanke, K.; Rolfs, C. Effects of Electron Screening on Low-Energy Fusion Cross Sections. *Z. Phys. A At. Nucl.* **1987**, *327*, 461–468. [CrossRef]
2. Engstler, S.; Krauss, A.; Neldner, K.; Rolfs, C.; Schröder, U.; Langanke, K. Effects of Electron Screening on the ^{3}He(d, p)^{4}He Low-Energy Cross Sections. *Phys. Lett. B* **1988**, *202*, 179–184. [CrossRef]
3. Bracci, L.; Fiorentini, G.; Mezzorani, G. A Dynamical Calculation of the Electron Shielding for D-d Fusion. *Phys. Lett. A* **1990**, *146*, 128–133. [CrossRef]
4. Rolfs, C.E.; Rodney, W.S. *Cauldrons in the Cosmos: Nuclear Astrophysics*, 1st ed.; University of Chicago Press: Chicago, IL, USA, 1988.
5. Aliotta, M.; Langanke, K. Screening Effects in Stars and in the Laboratory. *Front. Phys.* **2022**, *10*, 942726. [CrossRef]
6. Salpeter, E.-E. Electrons Screening and Thermonuclear Reactions. *Aust. J. Phys.* **1954**, *7*, 373. [CrossRef]
7. Adelberger, E.G.; García, A.; Robertson, R.G.H.; Snover, K.A.; Balantekin, A.B.; Heeger, K.; Ramsey-Musolf, M.J.; Bemmerer, D.; Junghans, A.; Bertulani, C.A.; et al. Solar Fusion Cross Sections. II. The pp Chain and CNO Cycles. *Rev. Mod. Phys.* **2011**, *83*, 195–245. [CrossRef]
8. Greife, U.; Gorris, F.; Junker, M.; Rolfs, C.; Zahnow, D. Oppenheimer-Phillips Effect and Electron Screening in D+ d Fusion Reactions. *Z. Phys. A Hadron. Nucl.* **1995**, *351*, 107–112. [CrossRef]
9. Yuki, H.; Sato, T.; Ohtsuki, T.; Yorita, T.; Aoki, Y.; Yamazaki, H.; Kasagi, J.; Ishii, K. Measurement of the D(d, p)T Reaction in Ti for 2.5 < Ed < 6.5 KeV and Electron Screening in Metal. *J. Phys. Soc. Jpn.* **1997**, *66*, 73–78.
10. Yuki, H.; Kasagi, J.; Lipson, A.G.; Ohtsuki, T.; Baba, T.; Noda, T.; Lyakhov, B.F.; Asami, N. Anomalous Enhancement of DD Reaction in Pd and Au/Pd/PdO Heterostructure Targets under Low-Energy Deuteron Bombardment. *JETP Lett.* **1998**, *68*, 823–829. [CrossRef]
11. Raiola, F.; Migliardi, P.; Gang, L.; Bonomo, C.; Gyürky, G.; Bonetti, R.; Broggini, C.; Christensen, N.E.; Corvisiero, P.; Cruz, J.; et al. Electron Screening in d(d,p)t for Deuterated Metals and the Periodic Table. *Phys. Lett. Sect. B Nucl. Elem. Part. High-Energy Phys.* **2002**, *547*, 193–199. [CrossRef]
12. Raiola, F.; Migliardi, P.; Gyürky, G.; Aliotta, M.; Formicola, A.; Bonetti, R.; Broggini, C.; Campajola, L.; Corvisiero, P.; Costantini, H.; et al. Enhanced Electron Screening in d(d,p)t for Deuterated Ta. *Eur. Phys. J. A* **2002**, *13*, 377–382. [CrossRef]
13. Raiola, F.; Gang, L.; Bonomo, C.; Gyürky, G.; Aliotta, M.; Becker, H.W.; Bonetti, R.; Broggini, C.; Corvisiero, P.; D'Onofrio, A.; et al. Enhanced Electron Screening in d(d,p)t for Deuterated Metals. *Eur. Phys. J. A* **2004**, *19*, 283–287. [CrossRef]
14. Raiola, F.; Burchard, B.; Fülöp, Z.; Gyürky, G.; Zeng, S.; Cruz, J.; Di Leva, A.; Limata, B.; Fonseca, M.; Luis, H.; et al. Electron Screening in d(d, p)t for Deuterated Metals: Temperature Effects. *J. Phys. G Nucl. Part. Phys.* **2005**, *31*, 1141. [CrossRef]
15. Ziegler, J.F.; Ziegler, M.D.; Biersack, J.P. SRIM – The Stopping and Range of Ions in Matter (2010). *Nucl. Instrum. Methods Phys. Res. B* **2010**, *268*, 1818–1823. [CrossRef]
16. Bonomo, C.; Fiorentini, G.; Fülöp, Z.; Gang, L.; Gyürky, G.; Langanke, K.; Raiola, F.; Rolfs, C.; Somorjai, E.; Strieder, F.; et al. Enhanced Electron Screening in d(d,p)t for Deuterated Metals: A Possible Classical Explanation. *Nucl. Phys. A* **2003**, *719*, C37–C42. [CrossRef]
17. Czerski, K.; Huke, A.; Heide, P.; Ruprecht, G. The 2H(d, p)3H Reaction in Metallic Media at Very Low Energies. *Europhys. Lett.* **2004**, *68*, 363. [CrossRef]
18. Kasagi, J.; Yuki, H.; Baba, T.; Noda, T.; Ohtsuki, T.; Lipson, A.G. Strongly Enhanced DD Fusion Reaction in Metals Observed for KeV D + Bombardment. *J. Phys. Soc. Jpn.* **2002**, *71*, 2881–2885. [CrossRef]
19. Czerski, K.; Huke, A.; Biller, A.; Heide, P.; Hoeft, M.; Ruprecht, G. Enhancement of the Electron Screening Effect for d + d Fusion Reactions in Metallic Environments. *Europhys. Lett.* **2001**, *54*, 449. [CrossRef]
20. Kaczmarski, M.; Czerski, K.; Weissbach, D.; Kilic, A.I.; Ruprecht, G.; Huke, A. Threshold Resonance Contribution to the Thick Target ^{2}H$(d,p)^3$H Reaction Yield. *Acta Phys. Pol. B* **2017**, *48*, 489. [CrossRef]

21. Targosz-Sleczka, N.; Czerski, K.; Kaczmarski, M.; Weissbach, D.; Kiliç, A.I.; Ruprecht, G.; Huke, A.; Policastro, S. Electron Screening Effect in Nuclear Reactions in Metallic and Gaseous Targets. *Acta Phys. Pol. B* **2018**, *49*, 675. [CrossRef]
22. Czerski, K.; Weissbach, D.; Kilic, A.I.; Ruprecht, G.; Huke, A.; Kaczmarski, M.; Targosz-Ślęczka, N.; Maass, K. Screening and Resonance Enhancements of the ^{2}H(d, p)^{3}H Reaction Yield in Metallic Environments. *EPL* **2016**, *113*, 22001. [CrossRef]
23. Czerski, K.; Targosz-Sleczka, N.; Kaczmarski, M. Deuteron-Deuteron Reaction Cross Sections at Very Low Energies. *Acta Phys. Pol. B* **2020**, *51*, 649. [CrossRef]
24. Czerski, K.; Huke, A.; Martin, L.; Targosz, N.; Blauth, D.; Górska, A.; Heide, P.; Winter, H. Measurements of Enhanced Electron Screening in D+d Reactions under UHV Conditions. *J. Phys. G Nucl. Part. Phys.* **2008**, *35*, 014012. [CrossRef]
25. Kowalska, A.; Czerski, K.; Horodek, P.; Siemek, K.; Kaczmarski, M.; Targosz-Ślęczka, N.; Valat, M.; Dubey, R.; Pyszniak, K.; Turek, M.; et al. Crystal Lattice Defects in Deuterated Zr in Presence of O and C Impurities Studied by PAS and XRD for Electron Screening Effect. *Materials* **2023**, *16*, 6255. [CrossRef]
26. Czerski, K. Deuteron-Deuteron Nuclear Reactions at Extremely Low Energies. *Phys. Rev. C* **2022**, *106*, L011601. [CrossRef]
27. Czerski, K.; Dubey, R.; Kaczmarski, M.; Kowalska, A.; Targosz-Ślęczka, N.; Das Haridas, G.; Valat, M. Indications of Electron Emission from the Deuteron-Deuteron Threshold Resonance. *Phys. Rev. C* **2024**, *109*, L021601. [CrossRef]
28. Bystritsky, V.M.; Bystritskii, V.M.; Dudkin, G.N.; Filipowicz, M.; Gazi, S.; Huran, J.; Kobzev, A.P.; Mesyats, G.A.; Nechaev, B.A.; Padalko, V.N.; et al. Measurement of Astrophysical S-Factors and Electron Screening Potentials for d(d,n)He3 Reaction in ZrD2, TiD2 and TaD0.5 Targets in the Ultralow Energy Region Using Plasma Accelerator. *Nucl. Phys. A* **2012**, *889*, 93–104. [CrossRef]
29. Prati, P.; Arpesella, C.; Bartolucci, F.; Becker, H.W.; Bellotti, E.; Broggini, C.; Corvisiero, P.; Fiorentini, G.; Fubini, A.; Gervino, G.; et al. Electron Screening in the D+3He Fusion Reaction. *Z. Phys. A Hadron. Nucl.* **1994**, *350*, 171–176. [CrossRef]
30. Engstler, S.; Raimann, G.; Angulo, C.; Greife, U.; Rolfs, C.; Schröder, U.; Somorjai, E.; Kirch, B.; Langanke, K. Test for Isotopic Dependence of Electron Screening in Fusion Reactions. *Phys. Lett. B* **1992**, *279*, 20–24. [CrossRef]
31. Junker, M.; Arpesella, C.; Bellotti, E.; Broggini, C.; Corvisiero, P.; D'Alessandro, A.; Fiorentini, G.; Fubini, A.; Gervino, G.; Greife, U.; et al. The Cross Section of ^{3}He(^{3}He,2p)^{4}He Measured at Solar Energies. *Nucl. Phys. B Proc. Suppl.* **1999**, *70*, 382–385. [CrossRef]
32. Bonetti, R.; Broggini, C.; Campajola, L.; Corvisiero, P.; D'alessandro, A.; Dessalvi, M.; D'onofrio, A.; Fubini, A.; Gervino, G.; Gialanella, L.; et al. First Measurement of the ^{3}He(^{3}He,2p)^{4}He Cross Section down to the Lower Edge of the Solar Gamow Peak. *Phys. Rev. Lett.* **1999**, *82*, 5205. [CrossRef]
33. Geist, W.H.; Brune, C.R.; Karwowski, H.J.; Ludwig, E.J.; Veal, K.D.; Hale, G.M. The ^{3}He(d→,p)^{4}He Reaction at Low Energies. *Phys. Rev. C* **1999**, *60*, 54003. [CrossRef]
34. Zavatarelli, S.; Corvisiero, P.; Costantini, H.; Moroni, P.G.P.; Prati, P.; Bonetti, R.; Guglielmetti, A.; Broggini, C.; Campajol, L.; Formicola, A.; et al. The D(^{3}He,p)^{4}He Fusion Reaction: Electron Screening Effect and Astrophysical S(E) Factor at Low Energies. *Nucl. Phys. A* **2001**, *688*, 514–517. [CrossRef]
35. Costantini, H.; Formicola, A.; Junker, M.; Bonetti, R.; Broggini, C.; Campajola, L.; Corvisiero, P.; D'Onofrio, A.; Fubini, A.; Gervino, G.; et al. Stopping Power, Electron Screening and the Astrophysical S(E) Factor of d(^{3}He,p)^{4}He Supported in Part by BMBF (06BO812) and Social European Fund.1. *Phys. Lett. B* **2000**, *482*, 43–49. [CrossRef]
36. Aliotta, M.; Raiola, F.; Gyürky, G.; Formicola, A.; Bonetti, R.; Broggini, C.; Campajola, L.; Corvisiero, P.; Costantini, H.; D'Onofrio, A.; et al. Electron Screening Effect in the Reactions ^{3}He(d,p)^{4}He and d(^{3}He,p)^{4}He☆☆Supported in Part by INFN, BMBF (06BO812), DFG (436UNG113-146) and OTKA (T025465). *Nucl. Phys. A* **2001**, *690*, 790–800. [CrossRef]
37. Typel, S.; Baur, G. Theory of the Trojan–Horse Method. *Ann. Phys.* **2003**, *305*, 228–265. [CrossRef]
38. Tumino, A.; Spartà, R.; Spitaleri, C.; Mukhamedzhanov, A.M.; Typel, S.; Pizzone, R.G.; Tognelli, E.; Degl'Innocenti, S.; Burjan, V.; Kroha, V.; et al. NEW DETERMINATION OF THE ^{2}H(d,p)^{3}H AND ^{2}H(d,n)^{3}He REACTION RATES AT ASTROPHYSICAL ENERGIES. *Astrophys. J.* **2014**, *785*, 96. [CrossRef]
39. Lipoglavšek, M.; Markelj, S.; Mihovilovič, M.; Petrovič, T.; Štajner, S.; Vencelj, M.; Vesić, J. Observation of Electron Emission in the Nuclear Reaction between Protons and Deuterons. *Phys. Lett. Sect. B Nucl. Elem. Part. High-Energy Phys.* **2017**, *773*, 553–556. [CrossRef]
40. Bystritsky, V.M.; Chumakov, D.K.; Dudkin, G.N.; Filipowicz, M.; Krylov, A.R.; Nechaev, B.A.; Nurkin, A.; Padalko, V.N.; Pen'kov, F.M.; Philippov, A.V.; et al. Determination of the Enhancement Factor and the Electron Screening Potential in the D(^{3}He,p)^{4}He Reaction Using TiD Targets. *Eur. Phys. J. A* **2020**, *56*, 60. [CrossRef]
41. Bystritsky, V.M.; Dudkin, G.N.; Krylov, A.R.; Nechaev, B.A.; Nurkin, A.; Padalko, V.N.; Varlachev, V.A.; Shuvalov, E.N.; Pen'kov, F.M.; Tuleushev, Y.Z.; et al. Investigation of the D(^{3}He, p)^{4}He Reaction on ZrD Targets in the Energy Region of 16–34 KeV. *Nucl. Phys. A* **2019**, *990*, 29–46. [CrossRef]
42. Schröder, U.; Engstler, S.; Krauss, A.; Neldner, K.; Rolfs, C.; Somorjai, E.; Langanke, K. Search for Electron Screening of Nuclear Reactions at Sub-Coulomb Energies. *Nucl. Inst. Methods Phys. Res. B* **1989**, *40–41*, 466–469. [CrossRef]
43. Engstler, S.; Raimann, G.; Angulo, C.; Greife, U.; Rolfs, C.; Schröder, U.; Somorjai, E.; Kirch, B.; Langanke, K. Isotopic Dependence of Electron Screening in Fusion Reactions. *Z. Phys. A Hadron. Nucl.* **1992**, *342*, 471–482. [CrossRef]
44. Musumarra, A.; Pizzone, R.G.; Blagus, S.; Bogovac, M.; Figuera, P.; Lattuada, M.; Milin, M.; Miljanić, Đ.; Pellegriti, M.G.; Rendić, D.; et al. Improved Information on the ^{2}H(^{6}Li,α)^{4}He Reaction Extracted via the "Trojan Horse" Method. *Phys. Rev. C* **2001**, *64*, 68801. [CrossRef]
45. Czerski, K.; Huke, A.; Bucka, H.; Heide, P.; Ruprecht, G.; Unrau, B. Subthreshold Resonance in ^{6}Li(d,α)^{4}He Reaction and Its Astrophysical Implications. *Phys. Rev. C* **1997**, *55*, 1517–1522. [CrossRef]

46. Kasagi, J.; Yuki, H.; Baba, T.; Noda, T.; Taguchi, J.; Shimokawa, M.; Galster, W. Strongly Enhanced Li + D Reaction in Pd Observed in Deuteron Bombardment on PdLix with Energies between 30 and 75 KeV. *J. Phys. Soc. Jpn.* **2004**, *73*, 608. [CrossRef]
47. Cruz, J.; Luis, H.; Fonseca, M.; Fülöp, Z.; Gyürky, G.; Raiola, F.; Aliotta, M.; Kettner, K.U.; Jesus, A.P.; Ribeiro, J.P.; et al. Experimental Study of Proton-Induced Nuclear Reactions in 6,7Li. *J. Phys. G Nucl. Part. Phys.* **2008**, *35*, 014004. [CrossRef]
48. Cruz, J.; Fülöp, Z.; Gyürky, G.; Raiola, F.; Di Leva, A.; Limata, B.; Fonseca, M.; Luis, H.; Schürmann, D.; Aliotta, M.; et al. Electron Screening in ^{7}Li(p,α)α and ^{6}Li(p,α)^{3}He for Different Environments. *Phys. Lett. Sect. B Nucl. Elem. Part. High-Energy Phys.* **2005**, *624*, 181–185. [CrossRef]
49. Zahnow, D.; Rolfs, C.; Schmidt, S.; Trautvetter, H.P. Low-Energy S(E) Factor of ^{9}Be(p,α)^{6}Li and ^{9}Be(p,d)^{8}Be. *Z. Für Phys. A Hadron. Nucl.* **1997**, *359*, 211–218. [CrossRef]
50. Lipoglavšek, M.; Čadež, I.; Markelj, S.; Pelicon, P.; Vavpetič, P. Electron Screening in the ^{1}H(7Li,α)^{4}He Reaction. *Eur. Phys. J. A* **2010**, *44*, 71–75. [CrossRef]
51. Vesic, J.; Cvetinovic, A.; Lipoglavsek, M.; Petrovic, T. Influence of Electronic Environment on Nuclear Reaction Rates. *Eur. Phys. J. A* **2014**, *50*, 153. [CrossRef]
52. Angulo, C.; Engstler, S.; Raimann, G.; Rolfs, C.; Schulte, W.H.; Somorjai, E. The Effects of Electron Screening and Resonances in (p, α) Reactions On10B And11B at Thermal Energies. *Z. Phys. A Hadron. Nucl.* **1993**, *345*, 231–242. [CrossRef]
53. Lamia, L.; Spitaleri, C.; Burjan, V.; Carlin, N.; Cherubini, S.; Crucillà, V.; Munhoz, M.G.; Santo, M.G.D.; Gulino, M.; Hons, Z.; et al. New Measurement of the ^{11}B(p,α_0)^{8}Be Bare-Nucleus S(E) Factor via the Trojan Horse Method. *J. Phys. G Nucl. Part. Phys.* **2012**, *39*, 015106. [CrossRef]
54. Spitaleri, C.; Lamia, L.; Puglia, S.M.R.; Romano, S.; La Cognata, M.; Crucillà, V.; Pizzone, R.G.; Rapisarda, G.G.; Sergi, M.L.; Del Santo, M.G.; et al. Measurement of the 10 KeV Resonance in the B 10 (p,A0) Be 7 Reaction via the Trojan Horse Method. *Phys. Rev. C Nucl. Phys.* **2014**, *90*, 035801. [CrossRef]
55. Fang, K.; Zhang, Q.; Chen, B.; Zhang, Z.; Wang, Q.; Wang, T.; Kasagi, J.; Hu, J.; Xu, S. Direct Measurement of Astrophysical Factor S(E) and Screening Potential for Be9(p,α)6Li Reaction at Low Energy. *Phys. Lett. B* **2018**, *785*, 262–267. [CrossRef]
56. Romano, S.; Lamia, L.; Spitaleri, C.; Li, C.; Cherubini, S.; Gulino, M.; La Cognata, M.; Pizzone, R.G.; Tumino, A. Study of The9Be(p, α)6Li Reaction via the Trojan Horse Method. *Eur. Phys. J. A* **2006**, *27*, 221–225. [CrossRef]
57. Wen, Q.-G.; Li, C.-B.; Zhou, S.-H.; Meng, Q.-Y.; Zhou, J.; Li, X.-M.; Hu, S.-Y.; Fu, Y.-Y.; Spitaleri, C.; Tumino, A.; et al. Trojan Horse Method Applied to ^{9}Be(p,α)^{6}Li at Astrophysical Energies. *Phys. Rev. C* **2008**, *78*, 35805. [CrossRef]
58. Kettner, K.U.; Becker, H.W.; Strieder, F.; Rolfs, C. High-Z Electron Screening: The Cases ^{50}V(p,n)^{50}Cr and ^{176}Lu(p,n)^{176}Hf. *J. Phys. G Nucl. Part. Phys.* **2006**, *32*, 489. [CrossRef]
59. Muir, H. Half-life heresy. *New Sci.* **2006**, *192*, 2574. [CrossRef]
60. Ujić, P.; de Oliveira Santos, F.; Lewitowicz, M.; Achouri, N.L.; Assié, M.; Bastin, B.; Borcea, C.; Borcea, R.; Buta, A.; Coc, A.; et al. Search for Superscreening Effects in a Superconductor. *Phys. Rev. Lett.* **2013**, *110*, 32501. [CrossRef]
61. Cvetinovic, A.; Lipoglavsek, M.; Markelj, S.; Vesic, J. Molecular Screening in Nuclear Reactions. *Phys. Rev. C Nucl. Phys.* **2015**, *92*, 065801. [CrossRef]
62. Cvetinović, A.; Đeorđić, D.; Guardo, G.L.; Kelemen, M.; La Cognata, M.; Lamia, L.; Markelj, S.; Mikac, U.; Pizzone, R.G.; Schwarz-Selinger, T.; et al. Electron Screening in Palladium. *Phys. Lett. Sect. B Nucl. Elem. Part. High-Energy Phys.* **2023**, *838*, 137684. [CrossRef]
63. Bencze, G. Electron Screening Effects in Low-Energy Fusion Reactions. *Nucl. Phys.* **1989**, *492*, 459–472. [CrossRef]
64. Salzmann, D.; Hass, M. Deuterium-Deuterium Nuclear Cross-Sections in Insulator and Metallic Environments. *Eur. Phys. J. A* **2008**, *36*, 359–364. [CrossRef]
65. Shoppa, T.D.; Koonin, S.E.; Langanke, K.; Seki, R. One- and Two-Electron Atomic Screening in Fusion Reactions. *Phys. Rev. C* **1993**, *48*, 837–840. [CrossRef]
66. Shoppa, T.D.; Jeng, M.; Koonin, S.E.; Langanke, K.; Seki, R. Electron Screening in Molecular Fusion Reactions. *Nucl. Phys. A* **1996**, *605*, 387–402. [CrossRef]
67. Huke, A.; Czerski, K.; Chun, S.M.; Biller, A.; Heide, P. Quantum Mechanical Ab Initio Simulation of the Electron Screening Effect in Metal Deuteride Crystals. *Eur. Phys. J. A* **2008**, *35*, 243–252. [CrossRef]
68. Czerski, K.; Huke, A.; Heide, P.; Ruprecht, G. Experimental and Theoretical Screening Energies for the ^{2}H(d, p) ^{3}H Reaction in Metallic Environments. *Eur. Phys. J. A* **2006**, *27*, 83–88. [CrossRef]
69. Carraro, C.; Schafer, A.; Koonin, S.-E. Dynamic Screening of Thermonuclear Reactions. *Astrophys. J.* **1988**, *331*, 565. [CrossRef]
70. Iliadis, C. Laboratory Electron Screening in Nuclear Resonance Reactions. *Phys. Rev. C* **2023**, *107*, 44610. [CrossRef]
71. Langanke, K.; Shoppa, T.D.; Barnes, C.A.; Rolfs, C. Energy Loss, Electron Screening and the Astrophysical ^{3}He(d, p)^{4}He Cross Section. *Phys. Lett. B* **1996**, *369*, 211–214. [CrossRef]
72. Bertulani, C.A. Electronic Stopping in Astrophysical Fusion Reactions. *Phys. Lett. B* **2004**, *585*, 35–41. [CrossRef]
73. Zylstra, A.B.; Herrmann, H.W.; Johnson, M.G.; Kim, Y.H.; Frenje, J.A.; Hale, G.; Li, C.K.; Rubery, M.; Paris, M.; Bacher, A.; et al. Using Inertial Fusion Implosions to Measure the T+^{3}He Fusion Cross Section at Nucleosynthesis-Relevant Energies. *Phys. Rev. Lett.* **2016**, *117*, 35002. [CrossRef] [PubMed]
74. Zylstra, A.B.; Herrmann, H.W.; Kim, Y.H.; McEvoy, A.; Frenje, J.A.; Johnson, M.G.; Petrasso, R.D.; Glebov, V.Y.; Forrest, C.; Delettrez, J.; et al. ^{2}H(p,γ)^{3}He Cross Section Measurement Using High-Energy-Density Plasmas. *Phys. Rev. C* **2020**, *101*, 42802. [CrossRef]

75. Zamfir, V.; Tanaka, K.; Ur, C. Extreme Light Infrastructure Nuclear Physics (ELI-NP). *Europhys. News* **2019**, *50*, 23–25. [CrossRef]
76. Schury, D.; Méry, A.; Ramillon, J.M.; Adoui, L.; Chesnel, J.-Y.; Lévy, A.; Macé, S.; Prigent, C.; Rangama, J.; Rousseau, P.; et al. The Low Energy Beamline of the FISIC Experiment: Current Status of Construction and Performance. *J. Phys. Conf. Ser.* **2020**, *1412*, 162011. [CrossRef]
77. Bruno, C.G.; Marsh, J.J.; Davinson, T.; Woods, P.J.; Black, P.; Bräuning-Demian, A.; Glorius, J.; Grant, A.; Hall, O.; Headspith, A.; et al. CARME—The CRYRING Array for Reaction MEasurements: A New Approach to Study Nuclear Reactions Using Storage Rings. *Nucl. Instrum. Methods Phys. Res. A* **2023**, *1048*, 168007. [CrossRef]
78. Bertulani, C.A.; Spitaleri, C. Nuclear Clustering and the Electron Screening Puzzle. *EPJ Web Conf.* **2017**, *165*, 02002. [CrossRef]
79. Spitaleri, C.; Bertulani, C.A.; Fortunato, L.; Vitturi, A. The Electron Screening Puzzle and Nuclear Clustering. *Phys. Lett. B* **2016**, *755*, 275–278. [CrossRef]